Acta Oceanol. Sin., 2021, Vol. 40, No. 9, P. 23–32
https://doi.org/10.1007/s13131-021-1899-7
http://www.aosocean.com
E-mail: ocean2@hyxb.org.cn

Pore-water geochemistry in methane-seep sediments of the Makran accretionary wedge off Pakistan: Possible link to subsurface methane hydrate

Xianrong Zhang[1, 2], Jianming Gong[1, 2], Zhilei Sun[1, 2*], Jing Liao[1, 2*], Bin Zhai[1, 2], Libo Wang[1, 2], Xilin Zhang[1, 2], Cuiling Xu[1, 2], Wei Geng[1, 2]

[1] Key Laboratory of Gas Hydrate of Ministry of Natural Resources, Qingdao Institute of Marine Geology, Qingdao 266071, China

[2] Evaluation and Detection Technology Laboratory for Marine Mineral Resources, Pilot National Laboratory for Marine Science and Technology (Qingdao), Qingdao 266237, China

Received 21 May 2020; accepted 18 September 2020

Abstract

Cold seeps are pervasive along the continental margin worldwide, and are recognized as hotspots for elemental cycling pathway on Earth. In this study, analyses of pore water geochemical compositions of one ~400 cm piston core (S3) and the application of a mass balance model are conducted to assess methane-associated biogeochemical reactions and uncover the relationship of methane in shallow sediment with gas hydrate reservoir at the Makran accretionary wedge off Pakistan. The results revealed that approximately 77% of sulfate is consumed by the predominant biogeochemical process of anaerobic oxidation of methane. However, the estimated sulfate-methane interface depth is ~400 cm below sea floor with the methane diffusive flux of 0.039 mol/(m^2·a), suggesting the activity of methane seepage. Based on the $\delta^{13}C_{DIC}$ mass balance model combined with the contribution proportion of different dissolved inorganic carbon sources, this study calculated the $\delta^{13}C$ of the exogenous methane to be –57.9‰, indicating that the exogenous methane may be a mixture source, including thermogenic and biogenic methane. The study of pore water geochemistry at Makran accretionary wedge off Pakistan may have considerable implications for understanding the specific details on the dynamics of methane in cold seeps and provide important evidence for the potential occurrence of subsurface gas hydrate in this area.

Key words: Makran accretionary wedge, methane-seep, pore water geochemistry, anaerobic oxidation of methane

Citation: Zhang Xianrong, Gong Jianming, Sun Zhilei, Liao Jing, Zhai Bin, Wang Libo, Zhang Xilin, Xu Cuiling, Geng Wei. 2021. Pore-water geochemistry in methane-seep sediments of the Makran accretionary wedge off Pakistan: Possible link to subsurface methane hydrate. Acta Oceanologica Sinica, 40(9): 23–32, doi: 10.1007/s13131-021-1899-7

1 Introduction

Cold seeps associated with natural gas hydrate are common and unique geological features, which are widely observed on both active and passive continental margins (Kvenvolden, 1993; Milkov, 2004; Skarke et al., 2014; Mau et al., 2017) and characterized by strong spatial and temporal variations in fluid flux. In these systems, methane-rich fluids pass through the sediment-seawater interface and discharge into seawater; ultimately, a fraction of the methane potentially reaches the atmosphere (Boetius and Wenzhöfer, 2013; Feng, et al., 2018; Ceramicola et al., 2018). Although seeps are heterogeneous both in time and space, they are considered to be hotspots of element cycling on Earth, representing an area that is typified by various biogeochemical processes, and thus commonly sustaining unique oasis-type ecosystems at the seafloor (Dickens, 2003; Boetius and Wenzhöfer, 2013; Suess, 2018; Crémière et al., 2016).

Geochemical composition of pore water provides the most straightforward and important signals for seafloor cold seep fluid activities and the biogeochemical processes associated with sulfate consumption. When the upward methane driven by buoyancy and pressure gradient meets the downward diffusion of sulfate, methane is consumed via anaerobic oxidation of methane (AOM: $CH_4+SO_4^{2-}\rightarrow HCO_3^-+HS^-+H_2O$) (Boetius et al., 2000; Reeburgh, 2007). Generally, AOM consumes up to nearly 90% of the total methane generated in the sediment, which reduces the release of methane to the hydrosphere and atmosphere (Reeburgh, 2007; Borowski et al., 1996). Besides that, organoclastic sulfate reduction (OSR: $2CH_2O+SO_4^{2-}\rightarrow 2HCO_3^-+H_2S$) also profoundly contributes to dissolved sulfate consumption and has a pivotal effect on the early diagenesis processes of marine sediments (Berner, 1980). Both AOM and OSR increase the concentration of dissolved inorganic carbon (DIC) concentration and the alkalinity of pore waters (Boetius et al., 2000). However, the DIC derived from AOM usually has an anomaly depleted ^{13}C feature, which is obviously different from OSR (Haese et al., 2003; Mazumdar et al., 2014; Solomon et al., 2014; Hu et al., 2015).

Foundation item: The National Natural Science Foundation of China under contract Nos 41606087, 91858208, and 42076069; the Taishan Scholar Special Experts Project under contract No. TS201712079; the National Key Basic Research and Development Program of China under contract No. 2017YFC0307704; the Marine Geological Survey Program of China Geological Survey under contract Nos DD20190518 and DD20190819.

*Corresponding author, E-mail: zhileisun@yeah.net; qdliaojing@gmail.com

Therefore, the changing concentrations of sulfate (SO_4^{2-}), DIC, as well as the $\delta^{13}C$ of DIC are diagnostic indicators to distinguish the relative contributions of AOM and OSR (Masuzawa et al., 1992; Chen et al., 2010; Solomon et al., 2014; Feng et al., 2018). In addition, these reactions in cold seeps, including AOM, OSR, precipitation of authigenic carbonate, etc., changes in the downcore profiles of pore-water species, i.e., SO_4^{2-}, CH_4, DIC, TA, Ca^{2+}, etc. Thus, pore-water geochemistry is of great importance in understanding and identifying the complex biogeochemical processes acting in cold seep.

Methane seepages and gas emissions are pervasive and vigorous on the continental slope of the Makran accretionary wedge off Pakistan (von Rad et al., 1996, 2000; Delisle and Berner, 2002; Fischer et al., 2009, 2013). First evidences of anomaly gas concentrations in sediments were found during seismic investigations of bright spots (White, 1977). Then, high-resolution multichannel seismic investigation indicates that bottom simulating with reversed polarity (BSR) compared with the seafloor reflection marking the lower boundary of the gas hydrate stability zone were identified at a depth of approximately 500–800 m below sea floor throughout the continental slope (Minshull and White, 1989; von Rad et al., 2000). Furthermore, high methane concentration anomalies in water column, seep-associated authigenic carbonate, as well as chemosynthetic clams were discovered in the 1990s (von Rad et al., 1996, 2000). Additionally, some works on chemical compositions of pore water and the methane seepages activity in the cold seeps were conducted (Fischer et al., 2009, 2011). However, besides cold seepage on the continental slope (von Rad et al., 1996, 2000), a series of mud volcanoes were discovered on the shelf close to the coast (Delisle et al., 2002), on land (Ellouz-Zimmermann et al., 2008; Kassi et al., 2014), and seaward of the Makran accretionary wedge (Wiedicke et al., 2001). Therefore, it is ideal area for exploring the methane seepages activity and the associated biogeochemical processes.

Here, this study presented the pore water geochemistry characteristic of a piston core (S3) collected from the Makran accretionary wedge off Pakistan. Geochemical characteristics of the chemical constituents (Cl^-, SO_4^{2-}, NH_4^+, I^-, K^+, Na^+, Mg^{2+}, Ca^{2+}, Sr and DIC) in combination with $\delta^{13}C_{DIC}$ were determined to characterize the methane seepages and methane-related biogeochemical processes in this area. Furthermore, an isotope mass balance model for DIC and $\delta^{13}C_{DIC}$ was used to discuss the methane sources and its association with the local gas hydrate system.

2 Geological setting

The accretionary wedge of the Makran subduction zone was formed when thick sediments were scraped from the Arabian Plat oceanic crust that was subducted beneath the continental Eurasian Plate. Subduction and accretion have probably been initiated since approximately the Paleocene (Platt et al., 1988) and Eocene (Byrne et al., 1992), respectively. The modern Makran accretionary prism developed in the Late Miocene (Platt et al., 1985, 1988).

The accretionary wedge is characterized by an extremely low angle of subduction (<2°), moderate convergence rate (~4 cm/a), ultra-width (>500 km) of the accretionary complex, and a remarkably thick sediment (>7 km) as a result of high terrigenous sedimentation (~0.2 m/ka to <1 m/ka) (White, 1982). The extension of the total slightly arcuate Makran accretionary wedge is about 800 km from east to west (Pakistan-Iran). The submarine segment of the accretionary complex has formed the convergent Makran continental margin off Pakistan, which is characterized by a narrow shelf (generally <25 km wide) and a steep continental slope (~ 90 km wide), and leaded to the Oman abyssal plain. A series of frontally accreted imbricated thrust slices cut by erosive submarine canyons developed on the continental slope, and expressed as long, narrow, and steep accretionary ridges separated by ponded slope basins (Kukowski et al., 2001).

3 Sampling and methods

3.1 *Sampling*

A piston core (S3) was collected near the seep site Flare-3 reported by Römer et al. (2012) in the Makran accretionary area off Pakistan during the comprehensive environmental geologic survey of R/V *Shiyan 3* in December 2017 (Fig. 1). The core length is 365 cm. The pore water extraction was conducted at 5–20 cm intervals immediately after sediment core retrieval onboard using Rhizon samplers (Seeberg-Elverfeldt et al., 2005) with the aper-

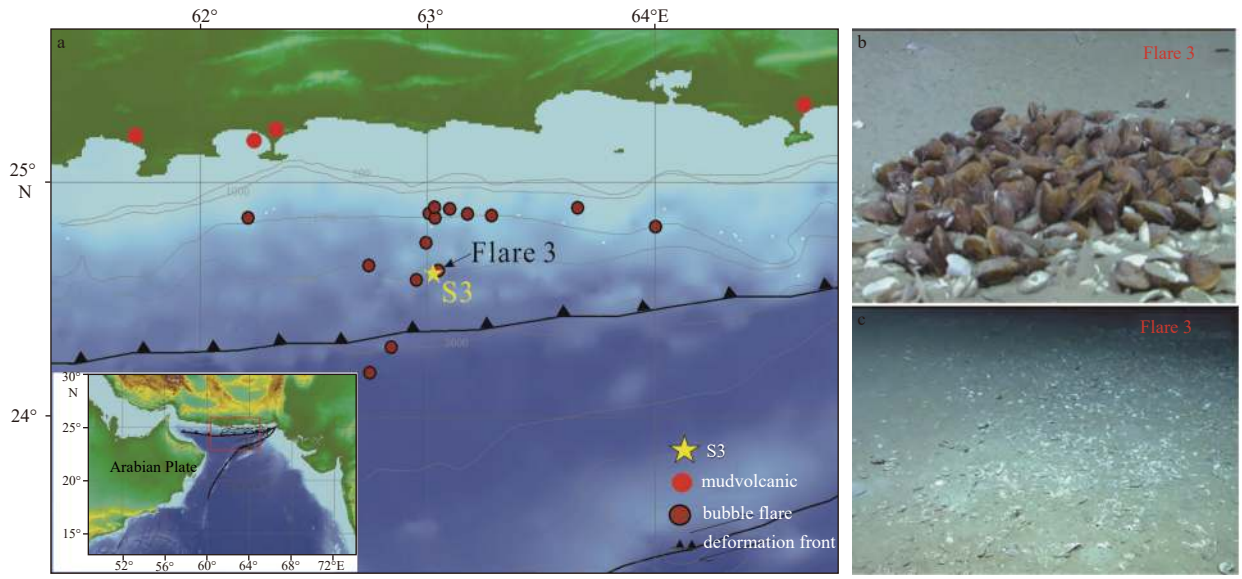

Fig. 1. Location of the sampling site at the Makran accretionary wedge off Pakistan (a), nests of living *Bathymodiolus* mussels at Flare 3 (Bohrmann, 2007) (b), and dead *calyptogena* clams scattered on the sea floor (Bohrmann, 2007) (c).

ture size of 0.2 μm. Pore water subsamples for the concentrations and isotope analysis of DIC were poisoned with saturated $HgCl_2$. All the pore water subsamples were stored at 4°C until further analysis.

3.2 *Methods*

The analyses of dissolved ion and stable isotopes were performed in the State Key Laboratory of Environmental Geochemistry, Third Institute of Oceanography (TIO), Ministry of Natural Resources (MNR, China). Before the analyses of the ion, the pore waters were diluted 1:100 with ultrapure water and filtered with 0.22 μm filter membrane. The dissolved ions concentrations of Cl^-, SO_4^{2-}, Br^-, Mg^{2+}, Ca^{2+}, K^+ and NH_4^+ in pore water were measured by ICS-1100 ion chromatography (Thermo Fisher Scientific, USA). The precision of replicate measurements was ±2% (n=5). Dissolved trace elements (Ba, Sr and I) were analyzed using high resolution Inductively Coupled Plasma Mass Spectrometry (ICP-MS). The analytical precisions were <5% for dissolved Ba and Sr, and <2% for I. Total alkalinity was measured by titration using Bruevich's method (Ivanenkov and Lyakhin, 1978), with the precision <2%.

Analyses of stable oxygen and hydrogen isotope compositions of pore water were determined by a high-temperature pyrolysis system directly-coupled to an isotope ratio mass spectrometer (Gehre and Strauch, 2003). Stable oxygen and hydrogen isotope compositions were calculated in δ-notation in per mill relative to the V-SMOW standard. The analytical precisions were ±0.4‰ for $\delta^{18}O$ and ±1.5‰ for δD.

The DIC concentrations and its stable carbon isotope were determined by continuous flow-isotope ratio mass spectrometer (CF-IRMS; Gasbench-Mat253, Thermo Fisher, USA). About 0.5 mL pore water sample was acidized with H_3PO_4. After 4 h reaction, the produced CO_2 was separated through a gas chromatographic column and transferred to a mass spectrometer for $\delta^{13}C$ determination. Stable isotopic values were presented with the Vienna-Pee Dee Belemnite (V-PDB) standard. The analytical precision was ±0.1‰ for $\delta^{13}C_{DIC}$.

4 Results

4.1 *Geochemical constituents of pore water*

Depth profiles of Cl^-,SO_4^{2-}, NH_4^+, I^-, Ca^{2+}, Mg^{2+}, Sr, Ba, and total alkalinity are shown in Fig. 2. The concentration of the conservative element Cl^- generally showed constant seawater-like values in the upper layer, and obvious fluctuations varying between 354 mmol/L and 574 mmol/L in the underlying layer. Sulfate concentrations linearly decreased with depth from near seawater-like values to the minimum value of 2.8 mmol/L at the bottom (Fig. 2). The profiles of alkaline earth elements (Mg^{2+} and Ca^{2+}) presented similar trend with sulfate, linearly decreased with the depth, and significant depletion of Ca^{2+} at the bottom of the core was noted with the minimum concentration of 1.4 mmol/L. In contrast, concentrations of NH_4^+ and the alkalinity in sediment increased with depth, and reached maximum values at the bottom, with the range from 0.7 mmol/L to 1.4 mmol/L for NH_4^+ and 4.3 mmol/L to 15.19 mmol/L for alkalinity.

4.2 *Profiles of DIC concentration and $\delta^{13}C$*

The profiles of DIC concentration and $\delta^{13}C_{DIC}$ are presented in Fig. 3. The DIC concentration generally increased from 2.2 mmol/L at the uppermost part of the core to 7.59 mmol/L at 365 cm below sea floor. The $\delta^{13}C_{DIC}$ decreased with the depth, from –10.5‰ to –31.0‰.

4.3 *Stable oxygen isotopes composition of pore water*

The downcore profile of the $\delta^{18}O$ is shown in Fig. 4. The $\delta^{18}O$ showed a variation range between –4.5‰ and –0.4‰, with prominent increase in the interval of about 290-310 cm below sea floor, corresponding to the decrease of Cl^-.

5 Discussion

5.1 *Potential occurrence of gas hydrate*

It is believed that the appearance of BSR can represent the base of the gas hydrate stability zone as a result of the acoustic impedance contrast between the overlying deposited gas hydrate and the underlying free gas layer (Shipley et al., 1979; Hyndman and Spence, 1992; Mazumdar et al., 2014). It can also occur due to the occurrence of small amounts of free gas below the gas hydrate stability zone with negligible presence of gas hydrate (Hyndman and Spence, 1992). The existence of high amplitude reflectors beneath the BSR reveals the presence of gas-charged sediments. According to previous seismic studies, the BSRs are widespread on the Makran accretionary wedge (Minshull and White, 1989; Minshull et al., 1992; von Rad et al., 2000; Sain et al., 2000; Shoar et al., 2014). In addition, the presence of gas hydrates and free-gas across the BSR in the Makran offshore are confirmed by the seismic characteristics, such as the blanking, instantaneous frequency and reflection strength (Ojha and Sain, 2009), and the velocity anomaly (Sain et al., 2000). In this study, the well-developed BSR with obviously reversed polarity was present in the seismic profile (Fig. 5), which may be related to the base of the gas hydrate stability zone and may define the phase boundary between gas hydrate-bearing sediments. In other words, there may be natural gas hydrate underlying/near our sampling site. In addition, several high angle fault rupture disrupting the overburden sediment can be clearly observed in the seismic reflection profiles (Fig. 5). Therefore, fluid associated with dissociation of gas hydrate may migrate through fracture to the shallow sediment. This assumption was supported by pore water anomalies as explained in the following.

Low chloride fluids at Site S3 (Fig. 4) in comparison with seawater are observed at the lower part (between 290 m and 310 m below sea floor), corresponding with positive peak in and $\delta^{18}O$ (Fig. 4). That can be attributed to the dissociation of gas hydrate and dehydration of clay minerals. However, the reaction clay mineral dehydration can be excluded since the feature of typical clay mineral transformation, i.e., Na^+ enrichment and K^+ depletion (Hesse, 2003), was not observed in Core S3 (Fig. 2). Cl^- concentrations and $\delta^{18}O$ anomalies in pore water have been reported in a number of gas hydrate-bearing sediments, e.g., the Blake Ridge (Borowski, 2004), the Nankai Trough (Toki et al., 2004), the Cascadia margin (Egeberg and Dickens, 1999; Torres et al., 2004), the Barbados Ridge (Kastner et al., 1990), the Black Sea (Reitz et al., 2011) and the South China Sea (Luo et al., 2014). Due to the salt exclusion and preferentially retain the heavier isotope ^{18}O in gas hydrates when they crystallize, the pore fluids could be additionally diluted by fresh water when gas hydrate dissociation. That result in the excursion of Cl^- concentration from baseline accompanied by the increase of pore water $\delta^{18}O$ (Egeberg and Dickens, 1999; Hesse, 2003; Ussler and Paull, 1995; Wallmann et al., 2006; Torres et al., 2004; Wu et al., 2013). Previous studies found that gas hydrates are occurred widely in Makran accretionary wedge off Pakistan, even at the depth of a few centimeters at Site Flare 2 (Bohrmann, 2008) which was not far from our station.

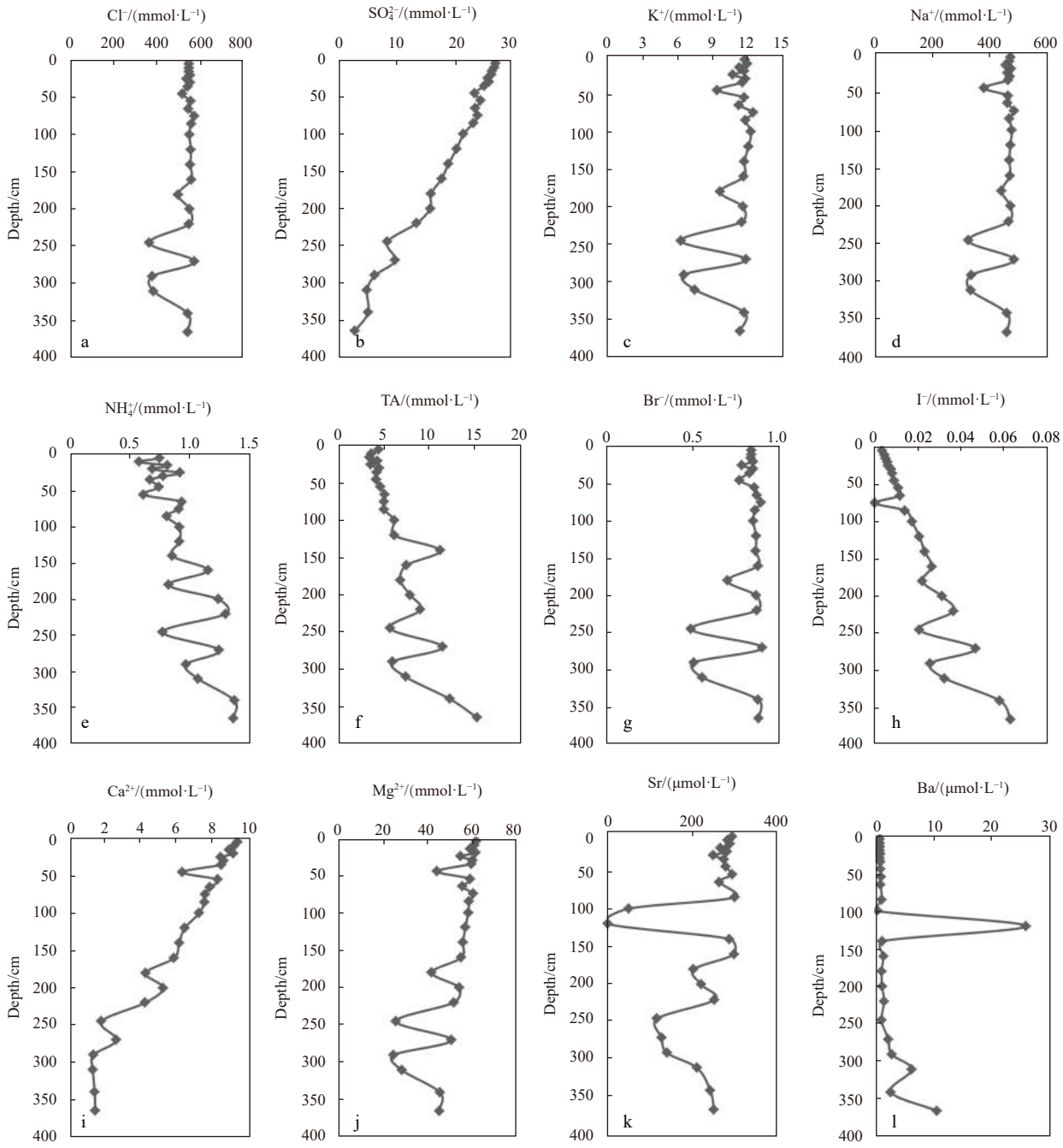

Fig. 2. Concentrations of major components in pore water of the Makran accretionary wedge off Pakistan.

Therefore, this study attributes the pore water anomalies to gas hydrate dissociation, which mean that gas hydrate may present underlying or near the studied sedimentary section.

Additionally, this study found that the $\delta^{18}O$ at Site S3 showed relatively negative values, which also has been found at ODP Site 1146 in the South China Sea and Nankai accretionary prism (Toki et al., 2014; Zhu et al., 2006). Besides that, Himmler et al. (2015) documented anomalously low $\delta^{18}O$ in the seep carbonates in the oxygen-minimum zone of the Makran accretionary wedge off Pakistan, which were attributed to ^{18}O-depleted fluids deriving the from formation of gas hydrate. Similarly, Site S3 is also situated in the oxygen-minimum zone with complicated deposition environment and vigorous seismicity (Fischer et al., 2013). Therefore, this study infers that the negative $\delta^{18}O$ background value may have been affected by the formation of gas hydrate or a complex fluid, but this need to be further studied.

5.2 *Sulfate reduction of Makran accretionary wedge*

In marine sediments, downward diffusing sulfate is considered as the major acceptors for the anaeraobic oxidation of methane and organic matter through microbially mediated processes: OSR (Berner, 1980) and AOM (Reeburgh, 1976; Boetius et al., 2000). Both of the sulfate reduction processes result in an enhanced DIC accumulation in pore water. For Core S3, the sulfate concentrations rapidly decrease with depths, and the total alkalinity values increase steadily down depth and reach maximum at

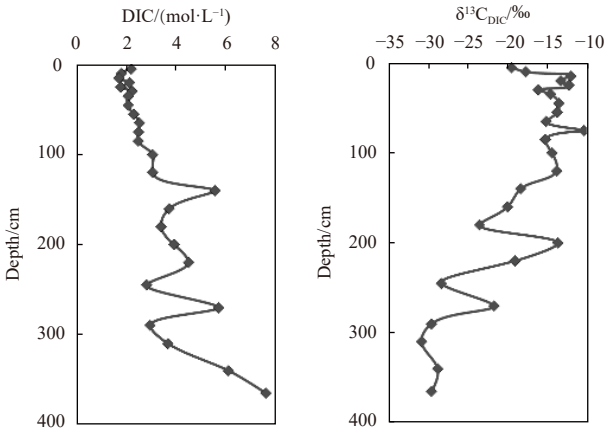

Fig. 3. Depth profiles of DIC concentration and $\delta^{13}C_{DIC}$ in Core S3.

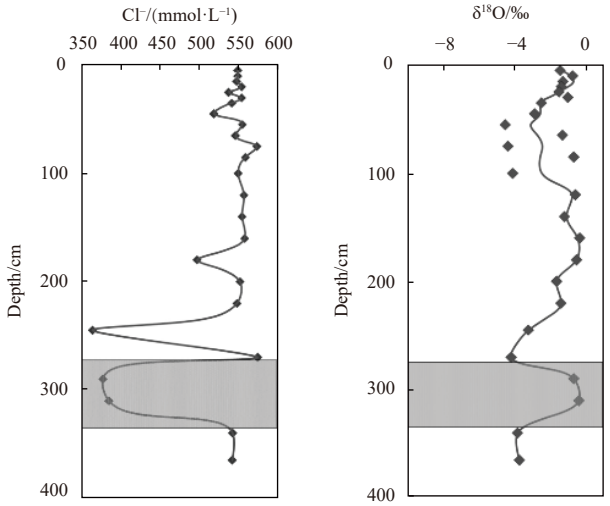

Fig. 4. Depth profiles of Cl^- concentration and $\delta^{18}O$ in the pore water of Site S3.

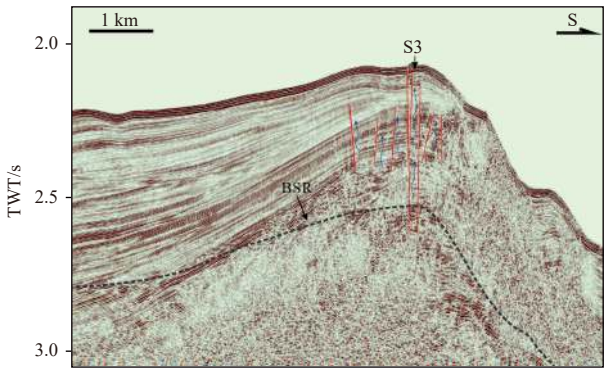

Fig. 5. Multi-channel seismic data in the studied area just beneath the sampling site highlighting the presence of bottom simulating with reversed polarity (BSR) in the study area. Red lines represent the high angle faults.

the bottom of the core (Fig. 2). This indicates the intensive microbial activities and actively sulfate reduction in the sediments.

NH_4^+ in pore water is the available candidate to evaluate the decomposition of organic matter, as their concentrations depend on the amount of buried organic matter and its degradation rate (Muramatsu and Wedepohl, 1998; Graca et al., 2006; Tomaru et al., 2009). NH_4^+ in pore water is produced via decomposition of the nitrogen-bearing organic matter, which has been documented to be stoichiometrically related to sulfate reduction (Henrichs and Reeburgh, 1987; Berner et al., 1970). In this study, NH_4^+ in sediment near-linearly increased with the depth, and ranged from 0.7 mmol/L to 1.4 mmol/L, pointing to relatively high rate degradations of organic matter. The cross-plots of the concentrations of SO_4^{2+} versus NH_4^+ yield correlation coefficient of 0.53 for Site S3 (Fig. 6), similar to others sites of the cold seeps in the ocean, where sulfate reduction is associated with organic matter degradation (Ye et al., 2016; Yang et al., 2013; Reitz et al., 2011; Mazumdar et al., 2014; Xu et al., 2018). On the other hand, relatively higher NH_4^+ than the upper part probably indicates that there may be a source from the organic matter degradation in the depth sediments rich in labile organic matter beneath the core (i.e., ex-situ origin; Mazumdar et al., 2014; Xu et al., 2018).

However, the quasi-linear shape sulfate profile and high alkalinity reflected a high AOM rate associated with high diffusive methane fluxes (Fig. 2; Borowski et al., 1996, 2000; Yang et al., 2013). Accordingly, the ratios of corrected produced DIC ($\Delta DIC+\Delta Ca^{2+}+\Delta Mg^{2+}$) and reduced sulfate ($\Delta SO_4^{2-}$) in pore water are usually used to evaluate the relative contributions of OSR and AOM (Masuzawa et al., 1992; Chen et al., 2010; Hu et al., 2015). Data obtained from Core S3 between slopes of 2:1 and 1:1, with slope of 1.23:1 (Fig. 7), suggested that sulfate reduction is contributed from a mixture of both OSR and AOM (Masuzawa et al., 1992). Also, AOM is the predominant biogeochemistry process for sulfate reduction with the contributions of ~77% in this area, whereas the contributions of OSR to sulfate reduction are ~23%. Additionally, the depleted $^{13}C_{DIC}$ (−37.0‰V-PDB) (Fig. 3)

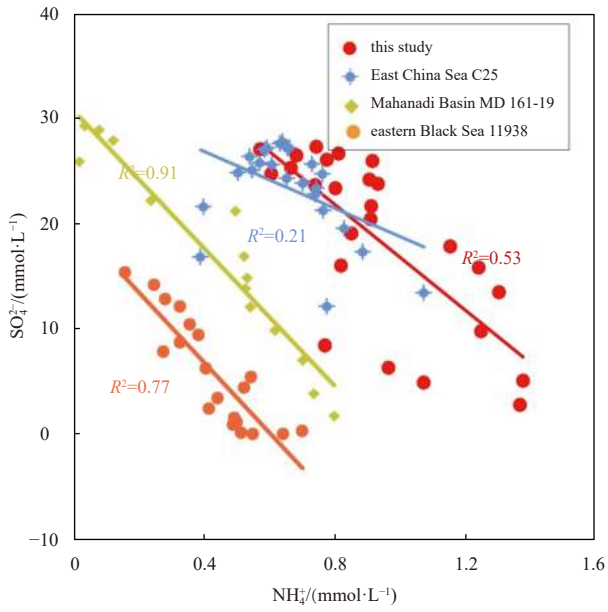

Fig. 6. Cross-plot of sulfate versus ammonium. A comparison was made among different locations of the other seas. The correlation coefficients were labeled closed to the fitting lines, together with corresponding annotations. Data for eastern Black Sea 11938 was taken from Reitz et al. (2011); Mahanadi Basin MD161-19 from Mazumdar et al. (2014); East China Sea from Xu et al. (2018).

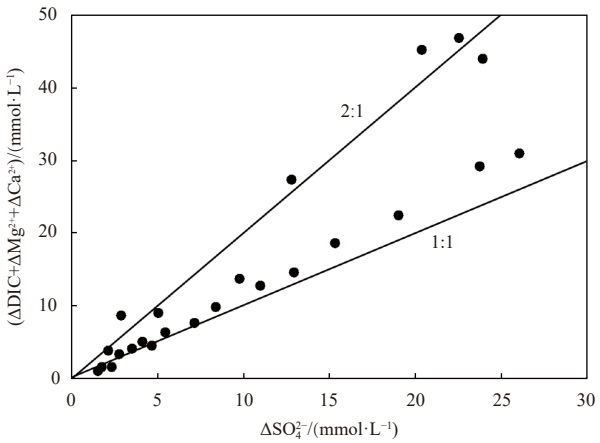

Fig. 7. Plot of sulfate concentration consumed versus DIC concentration produced and corrected for loss of Ca^{2+} concentration and Mg^{2+} concentration caused by authigenic carbonate precipitation. Diagonal lines indicate 1:1 and 2:1 ratios of DIC produced to sulfate consumed.

at 320 cm supports this observation.

5.3 *Methane flux and sources*

It was mentioned above that the linear SO_4^{2+} concentration gradient and $(\Delta DIC+\Delta Ca^{2+}+\Delta Mg^{2+})/\Delta SO_4^{2-}$ ratio allow us to identify the contribution of AOM, which is driven by upward migration of methane. Generally, the depth of sulfate-methane interface (SMI) is a typically indicator to imply relative magnitude of methane flux, with shallower SMI depths is corresponding to higher methane fluxes (Haese et al., 2003; Luff and Wallmann, 2003). At Site S3, the steep and near-linear sulfate concentration profile with the shallower SMI depth of ~4 m below sea floor, pointed to relatively high AOM rate with large upward methane flux. However, methane flux is difficult to be quantified by pore water methane concentration due to degassing of methane during core recovery. Nevertheless, it can be inferred from the flux of sulfate diffusing from seawater due to the 1:1 stoichiometric of methane and sulfate for AOM (Wallmann et al., 2006; Chuang et al., 2013; Luo et al., 2013; Mazumdar et al., 2014). The sulfate diffusive flux is estimated according to Fick's first law assuming steady state conditions (Berner, 1980):

$$J = -\varphi D_s \partial C/\partial x, \tag{1}$$

$$D_s = D_0/(1-\ln\varphi^2), \tag{2}$$

where J refers to the diffusive flux (mol/(m²·a)), φ refers to the porosity (this study assumed the porosity in our study to be 0.7) (Fischer et al., 2013), D_s refers to the sediment diffusion coefficient (m²/s), D_0 refers to the seawater diffusion coefficient, which can be calculated using equation presented by Boudreau (1997) with the bottom water temperature of 5°C. Sea-water sulfate D_0 at 5°C was 5.72×10^{-10} m²/s (Schulz, 2006). C and x indicate the sulfate concentration (mmol/L) and the sediment depth (m), respectively.

In this area, almost all of the upward-methane is consumed by AOM, which accounting for 77% of sulfate reduction; thus, the calculated methane flux is 77% of sulfate diffusive fluxes, which is equivalent to nearly 0.039 mol/(m²·a). However, compared with the flux from the Hydrate Site (Fischer et al., 2013) and the lower slope at the Makran accretionary wedge with a deeper SMI depth (ca. 6 m below sea floor) (unpublished data), it is higher than that. Additionally, compared with that from gas hydrate regions around the world, methane flux in the cold seep is notably higher than those in the northern South China Sea (0.014–0.035 mol/(m²·a) (Luo et al., 2013; Hu et al., 2015), and the Blake Ridge (0.02 mol/(m²·a), Borowski, 2004), whereas being lower than those from pockmarks and mud volcanos (Chen et al., 2010; Haese et al., 2003).

In general, methane is produced by two mechanisms in the marine sediments: microbial methane generated by CO_2-reduction or acetate fermentation, and thermogenic methane by thermal cracking of organic matter (Sackett, 1978; Whiticar, 1999). Thermogenic methane with the $\delta^{13}C$ more positive than −50‰ (Whiticar, 1999) is generally, but not exclusively, enriched in ^{13}C compared with bacterial methane (more negative than −60‰; Whiticar, 1999). Since $\delta^{13}C$ values of methane in Site S3 are unavailable, pore water DIC concentration and its $\delta^{13}C_{DIC}$ from the sulfate-methane transition zone (SMTZ) can be used to as an indicator for the source of methane (Kastner et al., 2008). Three possible sources of pore water DIC in marine sediments within the SMTZ are primarily included: (1) DIC diffusing from bottom seawater or seawater DIC being trapped within the sediment (SW); (2) generated via the OSR; (3) source from AOM. At SMTZ, methane is completely consumed, and carbon isotopic of DIC derived from AOM is the same as the methane oxidized. In order to distinguish sources of the pore water DIC in Site S3, this study use the mass balance model as follows (Borowski et al., 2000; Chen et al., 2010):

$$\delta^{13}C_{add} = X_{AOM}\times\delta^{13}C_{methane} + X_{SW}\times\delta^{13}C_{SW} + X_{OM}\times\delta^{13}C_{OM}, \tag{3}$$

where X refers to the proportion of DIC contributed to the entire DIC pool, $\delta^{13}C$ refers to the carbon isotopic constitution, and the subscripts AOM, SW and OM refer to DIC derived from the sources discussed above. This study estimated that the value of X_{SW} was 26.0% with $\delta^{13}C_{SW}$ of 0‰V-PDB. The $\delta^{13}C$ of sedimentary organic matter in Core S3 (−20.6‰V-PDB; unpublished data) was used for the $\delta^{13}C_{OM}$. The contributions estimated from DIC and sulfate stoichiometries were 57.0% for AOM, 17.0% for OM, and 26.0% for SW. In addition, the linear regression $\delta^{13}C\times DIC$ concentration versus DIC concentration has already been used to obtain DIC stable isotopic compositions added into the pore water DIC pool previously (e.g., Borowski et al., 2000; Ussler and Paull, 2008; Hu et al., 2018), thereby the calculated $\delta^{13}C_{add}$ is −33.1‰V-PDB (Fig. 8). Accordingly, the estimated $\delta^{13}C_{methane}$ in the Core S3 was −57.9‰V-PDB, indicating that the extraneous methane consumed by AOM has a mixed source including thermogenic and biogenic methane herein.

5.4 *Precipitation of authigenic carbonates*

Precipitation of authigenic carbonate is one of the striking phenomenon in cold seep system with fluid discharge, which can be observed by the consumption of pore water Ca^{2+}, Sr^{2+} and Mg^{2+} in shallow sediments (Gontharet et al., 2007; Cangemi et al., 2010; Haas et al., 2010; Hu et al., 2018; Luo et al., 2013; Nöthen and Kasten, 2011; Snyder et al., 2007). In Site S3, the concentrations of pore water Ca^{2+} and Mg^{2+} decreased significantly with the depth (Fig. 2), implying that authigenic carbonate may precipitate in the sediment. However, the concentration ratio of Mg/Ca increased from 6.6 in the near-surface sediment to approxim-

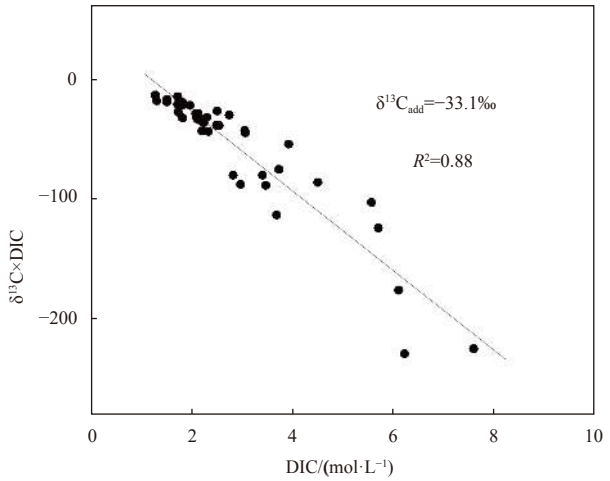

Fig. 8. The calculation of $\delta^{13}C_{add}$ using the linear regression of $\delta^{13}C\times DIC$ versus DIC concentration at Site S3.

ately 40 at the bottom of the core (Fig. 9), which indicate that high Mg/Ca carbonate mineral phase are precipitating. As presented in Fig. 10, weight ratios plot of pore water Sr/Ca and Mg/Ca in Site S3 are close to or fall on the composition line of high Mg-calcite, indicating that high Mg-calcite in the sediment is the predominant precipitation of authigenic carbonate mineral phase. Generally, aragonite is often observed to form preferentially in the environments with high sulfate concentrations and high fluxes of methane-rich fluids near the seafloor, whereas high Mg-calcite and dolomite precipitation may dominantly occur in

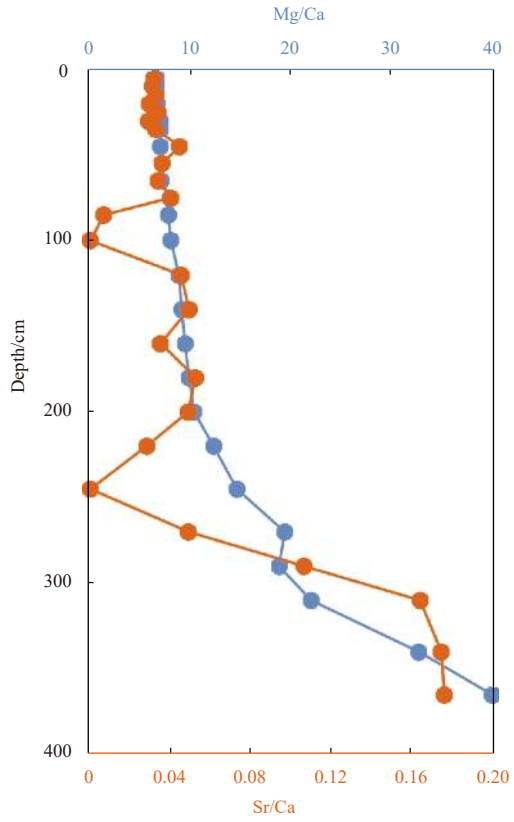

Fig. 9. Molar concentration ratios of Mg/Ca and Sr/Ca in Core S3. Both Mg/Ca and Sr/Ca ratios increase with depth obviously.

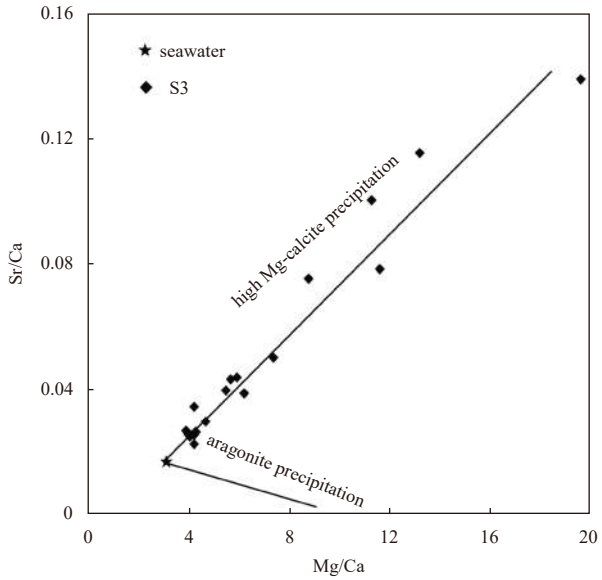

Fig. 10. Plot of Sr/Ca versus Mg/Ca (weight ratios) in pore waters. The Sr/Ca and Mg/Ca ratios of the precipitating aragonite and high Mg-calcite as well as seawater were taken from Bayon et al. (2007) and Nöthen and Kasten (2011).

the sediment within or beneath the SMI (Mazzini et al., 2006; Bayon et al., 2007). In contrast, our study found that high Mg-calcite precipitation has taken place in the shallow sediment of Site S3 above the SMI. This scenario suggests the downward shift of SMI due to the decreased upward methane flux, and may point to comparatively low activity seepage environment (methane diffusive flux, nearly 0.039 mol/(m²·a)) relative to the advection-dominated transport of methane.

6 Conclusions

Analysis of pore water geochemical characteristics of piston core (S3) sampled from shallow sediments at the Macron accretionary wedge off Pakistan revealed that the sulfate is consumed by both OSR and AOM. Proportion of sulfate consumed by the AOM is approximately 77%, which predominantly controls the sulfate concentration profiles. The near-linear sulfate profile, shallow SMI (~4 cm below sea floor) and methane flux toward the SMTZ (0.039 mol/(m²·a)) revealed the gas seepage activity in the study area. The calculated $\delta^{13}C$ of the external methane in Site S3 was to be –57.9‰ based on the mass balance model of DIC, indicating that the methane consumed by AOM are most likely a mixed source, including thermogenic and biogenic methane. The weight ratios of pore water Sr/Ca and Mg/Ca in Site S3 suggested that the predominant precipitation of authigenic carbonate was high Mg-calcite, which may point that this area is a relatively low-activity seepage environment, which is in accordance with the estimated methane diffusive flux.

Acknowledgements

We thank the captains and crew of the R/V *Shiyan 3* for their assistance in recovering the samples during the integrated environmental and geological expedition on the Macron accretionary wedge in December 2017.

References

Bayon G, Pierre C, Etoubleau J, et al. 2007. Sr/Ca and Mg/Ca ratios in Niger Delta sediments: implications for authigenic carbonate

genesis in cold seep environments. Marine Geology, 241(1–4): 93–109
Berner R A. 1980. Early Diagenesis: A Theoretical Approach. Princeton: Princeton University Press
Berner R A, Scott M R, Thomlinson C. 1970. Carbonate alkalinity in the pore waters of anoxic marine sediments. Limnology and Oceanography, 15(4): 544–549, doi: 10.4319/lo.1970.15.4.0544
Boetius A, Ravenschlag K, Schubert C J, et al. 2000. A marine microbial consortium apparently mediating anaerobic oxidation of methane. Nature, 407(6804): 623–626, doi: 10.1038/35036572
Boetius A, Wenzhöfer F. 2013. Seafloor oxygen consumption fuelled by methane from cold seeps. Nature Geoscience, 6(9): 725–734, doi: 10.1038/ngeo1926
Bohrmann G. 2008. Report and Preliminary Results of R/V *Meteor Cruise M74/3*, Fujairah Male, 30 October–28 November, 2007. Cold Seeps of the Makran Subduction Zone (Continental Margin of Pakistan). Bremen: Universität Bremen
Borowski W S, Çagatay N, Ternois Y, et al. 2000. Data report: carbon isotopic composition of dissolved CO_2, CO_2 gas, and methane, Blake-Bahama Ridge and northeast Bermuda Rise, ODP Leg 172. In: Keigwin L D, Rio D, Acton G D, et al., eds. Proceedings of the Ocean Drilling Program, Scientific Results, 172: 1–16, doi: 10.2973/odp.proc.sr.172.201.2000
Borowski W S, Paull C K, Ussler III W. 1996. Marine pore-water sulfate profiles indicate *in situ* methane flux from underlying gas hydrate. Geology, 24(7): 655–658, doi: 10.1130/0091-7613(1996)024<0655:MPWSPI>2.3.CO;2
Borowski W S. 2004. A review of methane and gas hydrates in the dynamic, stratified system of the Blake Ridge region, offshore southeastern North America. Chemical Geology, 205(3–4): 311–346
Boudreau B P. 1997. Diagenetic Models and Their Implementation: Modelling Transport and Reactions in Aquatic Sediments. Berlin: Springer
Byrne D E, Sykes L R, Davis D M. 1992. Great thrust earthquakes and aseismic slip along the plate boundary of the Makran Subduction Zone. Journal of Geophysical Research, 97(B1): 449–478, doi: 10.1029/91JB02165
Cangemi M, Di Leonardo R, Bellanca A, et al. 2010. Geochemistry and mineralogy of sediments and authigenic carbonates from the Malta Plateau, Strait of Sicily (Central Mediterranean): relationships with mud/fluid release from a mud volcano system. Chemical Geology, 276(3–4): 294–308
Ceramicola S, Dupré S, Somoza L, et al. 2018. Cold seep systems. In: Micallef A, Krastel S, Savini A, eds. Submarine Geomorphology. Cham: Springer, 367–387
Chen Yifeng, Ussler III W, Haflidason H, et al. 2010. Sources of methane inferred from pore-water $\delta^{13}C$ of dissolved inorganic carbon in pockmark G11, offshore Mid-Norway. Chemical Geology, 275(3–4): 127–138
Chuang Peichuan, Dale A W, Wallmann K, et al. 2013. Relating sulfate and methane dynamics to geology: accretionary prism offshore SW Taiwan. Geochemistry, Geophysics, Geosystems, 14(7): 2523–2545, doi: 10.1002/ggge.20168
Crémière A, Lepland A, Chand S, et al. 2016. Timescales of methane seepage on the Norwegian margin following collapse of the Scandinavian Ice Sheet. Nature Communications, 7(1): 11509, doi: 10.1038/ncomms11509
Delisle G, Berner U. 2002. Gas hydrates acting as cap rock to fluid discharge in the Makran accretionary prism?. In: Clift P D, Kroon D, Gaedicke C, et al., eds. The Tectonic and Climatic Evolution of the Arabian Sea Region. London: Geological Society, 137–146
Delisle G, von Rad U, Andruleit H, et al. 2002. Active mud volcanoes on-and offshore eastern Makran, Pakistan. International Journal of Earth Sciences, 91(1): 93–110, doi: 10.1007/s005310100203
Dickens G R. 2003. CLIMATE: a methane trigger for rapid warming?. Science, 299(5609): 1017–1017, doi: 10.1126/science.1080789
Egeberg P K, Dickens G R. 1999. Thermodynamic and pore water halogen constraints on gas hydrate distribution at ODP site 997 (Blake Ridge). Chemical Geology, 153(1–4): 53–79
Ellouz-Zimmermann N, Battani A, Deville E, et al. 2008. Impact of coeval tectonic and sedimentary-driven tectonics on the development of overpressure cells, on the sealing, and fluid migration—Petroleum potential and environmental risks of the Makran Accretionary Prism in Pakistan. Himalayan Journal of Sciences, 5(7): 50–51
Feng Dong, Qiu Jianwen, Hu Yu, et al. 2018. Cold seep systems in the South China Sea: an overview. Journal of Asian Earth Sciences, 168: 3–16, doi: 10.1016/j.jseaes.2018.09.021
Fischer D, Bohrmann G, Zabel M, et al. 2009. Geochemical zonation and characteristics of cold seeps along the Makran continental margin off Pakistan. In: EGU General Assembly. Vienna: EGU
Fischer D, Sahling H, Nöthen K, et al. 2011. Interaction between hydrocarbon seepage, chemosynthetic communities, and bottom water redox at cold seeps of the Makran accretionary prism: insights from habitat-specific pore water sampling and modeling. Biogeosciences, 9(6): 2013–2031
Fischer D, Mogollón J M, Strasser M, et al. 2013. Subduction zone earthquake as potential trigger of submarine hydrocarbon seepage. Nature Geoscience, 6(8): 647–651, doi: 10.1038/ngeo1886
Gehre M, Strauch G. 2003. High-temperature elemental analysis and pyrolysis techniques for stable isotope analysis. Rapid Communications in Mass Spectrom, 17(13): 1497–1503, doi: 10.1002/rcm.1076
Gontharet S, Pierre C, Blanc-Valleron M M, et al. 2007. Nature and origin of diagenetic carbonate crusts and concretions from mud volcanoes and pockmarks of the Nile deep-sea fan (eastern Mediterranean Sea). Deep-Sea Research Part II: Topical Studies in Oceanography, 54(11–13): 1292–1311
Graca B, Witek Z, Burska D, et al. 2006. Pore water phosphate and ammonia below the permanent halocline in the South-eastern Baltic Sea and their benthic fluxes under anoxic conditions. Journal of Marine Systems, 63(3–4): 141–154
Haas A, Peckmann J, Elvert M, et al. 2010. Patterns of carbonate authigenesis at the Kouilou pockmarks on the Congo deep-sea fan. Marine Geology, 268(1–4): 129–136
Haese R R, Meile C, Van Cappellen P. et al 2003. Carbon geochemistry of cold seeps: methane fluxes and transformation in sediments from Kazan mud volcano, eastern Mediterranean Sea. Earth and Planetary Science Letters, 212(3–4): 361–375
Henrichs S M, Reeburgh W S. 1987. Anaerobic mineralization of marine sediment organic matter: rates and the role of anaerobic processes in the oceanic carbon economy. Geomicrobiology Journal, 5(3–4): 191–237
Hesse R. 2003. Pore water anomalies of submarine gas-hydrate zones as tool to assess hydrate abundance and distribution in the subsurface: what have we learned in the past decade?. Earth-Science Reviews, 61(1–2): 149–179
Hu Yu, Feng Dong, Liang Qianyong, et al. 2015. Impact of anaerobic oxidation of methane on the geochemical cycle of redox-sensitive elements at cold-seep sites of the northern South China Sea. Deep-Sea Research Part II: Topical Studies in Oceanography, 122: 84–94, doi: 10.1016/j.dsr2.2015.06.012
Hu Yu, Luo Min, Chen Linying, et al. 2018. Methane source linked to gas hydrate system at hydrate drilling areas of the South China Sea: porewater geochemistry and numerical model constraints. Journal of Asian Earth Sciences, 168: 87–95, doi: 10.1016/j.jseaes.2018.04.028
Hyndman R D, Spence G D. 1992. A seismic study of methane hydrate marine bottom simulating reflectors. Journal of Geophysical Research, 97(B5): 6683–6698, doi: 10.1029/92JB00234
Ivanenkov V N, Lyakhin Y I. 1978. Determination of total alkalinity in seawater. In: Bordovsky O K, Ivanenkov V N, eds. Methods of Hydrochemical Investigations in the Ocean. Moscow: Nauka Publ, 110–114
Kassi A M, Khan S D, Bayraktar H, et al. 2014. Newly discovered mud volcanoes in the coastal belt of Makran, Pakistan—tectonic implications. Arabian Journal of Geosciences, 7(11): 4899–4909, doi: 10.1007/s12517-013-1135-7
Kastner M, Claypool G, Robertson G. 2008. Geochemical constraints on the origin of the pore fluids and gas hydrate distribution at

Atwater Valley and Keathley Canyon, northern Gulf of Mexico. Marine and Petroleum Geology, 25(9): 860–872, doi: 10.1016/j.marpetgeo.2008.01.022

Kastner M, Elderfield H, Martin J B, et al. 1990. Diagenesis and interstitial-water chemistry at the Peruvian continental margin-major constituents and strontium isotopes. In: Suess E, Von Huene R, eds. Proceedings of the Ocean Drilling Program, Scientific Results. College Station: Ocean Drilling Program, 413–440, doi: 10.2973/odp.proc.sr.112.144.1990

Kukowski N, Schillhorn T, Huhn K, et al. 2001. Morphotectonics and mechanics of the central Makran accretionary wedge off Pakistan. Marine Geology, 173(1–4): 1–19

Kvenvolden K A, Ginsburg G D, Soloviev V A. 1993. Worldwide distribution of subaquatic gas hydrates. Geo-Marine Letters, 13(1): 32–40, doi: 10.1007/BF01204390

Luff R, Wallmann K. 2003. Fluid flow, methane fluxes, carbonate precipitation and biogeochemical turnover in gas hydrate-bearing sediments at Hydrate Ridge, Cascadia Margin: numerical modeling and mass balances. Geochimica et Cosmochimica Acta, 67(18): 3403–3421, doi: 10.1016/S0016-7037(03)00127-3

Luo Min, Chen Linying, Tong Hongpeng, et al. 2014. Gas hydrate occurrence inferred from dissolved Cl^- concentrations and $\delta^{18}O$ values of pore water and dissolved sulfate in the shallow sediments of the pockmark field in southwestern Xisha Uplift, Northern South China Sea. Energies, 7(6): 3886–3899, doi: 10.3390/en7063886

Luo Min, Chen Linying, Wang Shuhong, et al. 2013. Pockmark activity inferred from pore water geochemistry in shallow sediments of the pockmark field in southwestern Xisha Uplift, northwestern South China Sea. Marine and Petroleum Geology, 48: 247–259, doi: 10.1016/j.marpetgeo.2013.08.018

Masuzawa T, Handa N, Kitagawa H, et al. 1992. Sulfate reduction using methane in sediments beneath a bathyal “cold seep” giant clam community off Hatsushima Island, Sagami Bay, Japan. Earth and Planetary Science Letters, 110(1–4): 39–50

Mau S, Römer M, Torres M E, et al. 2017. Widespread methane seepage along the continental margin off Svalbard—from Bjørnøya to Kongsfjorden. Scientific Reports, 7(1): 42997, doi: 10.1038/srep42997

Mazumdar A, Peketi A, Joao H M, et al. 2014. Pore-water chemistry of sediment cores off Mahanadi Basin, Bay of Bengal: possible link to deep seated methane hydrate deposit. Marine and Petroleum Geology, 49: 162–175, doi: 10.1016/j.marpetgeo.2013.10.011

Mazzini A, Svensen H, Hovland M, et al. 2006. Comparison and implications from strikingly different authigenic carbonates in a Nyegga complex pockmark, G11, Norwegian Sea. Marine Geology, 231(1–4): 89–102

Milkov A V. 2004. Global estimates of hydrate-bound gas in marine sediments: how much is really out there?. Earth-Science Reviews, 66(3–4): 183–197

Minshull T, White R. 1989. Sediment compaction and fluid migration in the Makran accretionary prism. Journal of Geophysical Research, 94(B6): 7387–7402, doi: 10.1029/JB094iB06p07387

Minshull T A, White R S, Barton P J, et al. 1992. Deformation at plate boundaries around the Gulf of Oman. Marine Geology, 104(1–4): 265–277

Muramatsu Y, Wedepohl K H. 1998. The distribution of iodine in the earth’s crust. Chemical Geology, 147(3–4): 201–216

Nöthen K, Kasten S. 2011. Reconstructing changes in seep activity by means of pore water and solid phase Sr/Ca and Mg/Ca ratios in pockmark sediments of the Northern Congo Fan. Marine Geology, 287(1–4): 1–13

Ojha M, Sain K. 2009. Seismic attributes for identifying gas-hydrates and free-gas zones: application to the Makran accretionary prism. Episodes, 32(4): 264–270, doi: 10.18814/epiiugs/2009/v32i4/003

Platt J P, Leggett J K, Alam S. 1988. Slip vectors and fault mechanics in the Makran accretionary wedge, Southwest Pakistan. Journal of Geophysical Research, 93(B7): 7955–7973, doi: 10.1029/JB093iB07p07955

Platt J P, Leggett J K, Young H, et al. 1985. Large-scale sediment underplating in the Makran accretionary prism, southwest Pakistan. Geology, 13(7): 507–511, doi: 10.1130/0091-7613(1985)13<507:LSUITM>2.0.CO;2

Reeburgh W S. 1976. Methane consumption in Cariaco Trench waters and sediments. Earth and Planetary Science Letters, 28(3): 337–344, doi: 10.1016/0012-821X(76)90195-3

Reeburgh W S. 2007. Oceanic methane biogeochemistry. Chemical Reviews, 107(2): 486–513, doi: 10.1021/cr050362v

Reitz A, Pape T, Haeckel M, et al. 2011. Sources of fluids and gases expelled at cold seeps offshore Georgia, eastern Black Sea. Geochimica et Cosmochimica Acta, 75(11): 3250–3268, doi: 10.1016/j.gca.2011.03.018

Römer M, Sahling H, Pape T, et al. 2012. Quantification of gas bubble emissions from submarine hydrocarbon seeps at the Makran continental margin (offshore Pakistan). Journal of Geophysical Research, 117(C10): C10015, doi: 10.1029/2011JC007424

Sackett W M. 1978. Carbon and hydrogen isotope effects during the thermocatalytic production of hydrocarbons in laboratory simulation experiments. Geochimica et Cosmochimica Acta, 42(6): 571–580, doi: 10.1016/0016-7037(78)90002-9

Sain K, Minshull T A, Singh S C, et al. 2000. Evidence for a thick free gas layer beneath the bottom simulating reflector in the Makran accretionary prism. Marine Geology, 164(1–2): 3–12

Schulz H D. 2006. Quantification of early diagenesis: dissolved constituents in pore water and signals in the solid phase. In: Schulz H D, Zabel M, eds. Marine Geochemistry. Berlin, Germany: Springer

Seeberg-Elverfeldt J, Schlüter M, Feseker T, et al. 2005. Rhizon sampling of porewaters near the sediment-water interface of aquatic systems. Limnology and Oceanography: Methods, 3(8): 361–371, doi: 10.4319/lom.2005.3.361

Shipley T H, Houston M H, Buffler R T, et al. 1979. Seismic evidence for widespread possible gas hydrate horizons on continental slopes and rises. AAPG Bulletin, 63(12): 2204–2213

Shoar B H, Javaherian A, Farajkhah N K, et al. 2014. Reflectivity template, a quantitative intercept-gradient AVO analysis to study gas hydrate resources—a case study of Iranian deep sea sediments. Marine and Petroleum Geology, 51: 184–196, doi: 10.1016/j.marpetgeo.2013.12.007

Skarke A, Ruppel C, Kodis M, et al. 2014. Widespread methane leakage from the sea floor on the northern us Atlantic margin. Nature Geoscience, 7(9): 657–661, doi: 10.1038/ngeo2232

Snyder G T, Hiruta A, Matsumoto R, et al. 2007. Pore water profiles and authigenic mineralization in shallow marine sediments above the methane-charged system on Umitaka Spur, Japan Sea. Deep-Sea Research Part II: Topical Studies in Oceanography, 54(11–13): 1216–1239

Solomon E A, Spivack A J, Kastner M, et al. 2014. Gas hydrate distribution and carbon sequestration through coupled microbial methanogenesis and silicate weathering in the Krishna-Godavari Basin, offshore India. Marine and Petroleum Geology, 58: 233–253, doi: 10.1016/j.marpetgeo.2014.08.020

Suess E. 2018. Marine cold seeps: background and recent advances. In: Wilkes H, ed. Hydrocarbons, Oils and Lipids: Diversity, Origin, Chemistry and Fate. Cham: Springer, 1–21

Toki T, Higa R, Ijiri A, et al. 2014. Origin and transport of pore fluids in the Nankai accretionary prism inferred from chemical and isotopic compositions of pore water at cold seep sites off Kumano. Earth, Planets and Space, 66(1): 137, doi: 10.1186/s40623-014-0137-3

Toki T, Tsunogai U, Gamo T, et al. 2004. Detection of low-chloride fluids beneath a cold seep field on the Nankai accretionary wedge off Kumano, South of Japan. Earth and Planetary Science Letters, 228(1–2): 37–47, doi: 10.1016/j.epsl.2004.09.007

Tomaru H, Fehn U, Lu Zunli, et al. 2009. Dating of dissolved iodine in pore waters from the gas hydrate occurrence offshore Shimokita Peninsula, Japan: ^{129}I results from the D/V *Chikyu* Shakedown Cruise. Resource Geology, 59(4): 359–373, doi: 10.1111/j.1751-3928.2009.00103.x

Torres M E, Wallmann K, Tréhu A M, et al. 2004. Gas hydrate growth,

methane transport, and chloride enrichment at the southern summit of Hydrate Ridge, Cascadia margin off Oregon. Earth and Planetary Science Letters, 226(1–2): 225–241

Ussler III W, Paull C K. 1995. Effects of ion exclusion and isotopic fractionation on pore water geochemistry during gas hydrate formation and decomposition. Geo-Marine Letters, 15(1): 37–44, doi: 10.1007/BF01204496

Ussler III W, Paull C K. 2008. Rates of anaerobic oxidation of methane and authigenic carbonate mineralization in methane-rich deep-sea sediments inferred from models and geochemical profiles. Earth and Planetary Science Letters, 266(3–4): 271–287

von Rad U, Berner U, Delisle G, et al. 2000. Gas and fluid venting at the makran accretionary wedge off Pakistan. Geo-Marine Letters, 20(1): 10–19, doi: 10.1007/s003670000033

von Rad U, Rösch H, Berner U, et al. 1996. Authigenic carbonates derived from oxidized methane vented from the Makran accretionary prism off Pakistan. Marine Geology, 136(1–2): 55–77

Wallmann K, Aloisi G, Haeckel M, et al. 2006. Kinetics of organic matter degradation, microbial methane generation, and gas hydrate formation in anoxic marine sediments. Geochimica et Cosmochimica Acta, 70(15): 3905–3927, doi: 10.1016/j.gca.2006.06.003

White R S. 1977. Seismic bright spots in the Gulf of Oman. Earth and Planetary Science Letters, 37(1): 29–37, doi: 10.1016/0012-821X(77)90143-1

White R S. 1982. Deformation of the Makran accretionary sediment prism in the Gulf of Oman (North-West Indian Ocean). In: Leggett J K, ed. Trench-Forearc Geology: Sedimentation and Tectonics on Modern and Ancient Active Plate Margins. London: Geological Society, 357–372

Wiedicke M, Neben S, Spiess V. 2001. Mud volcanoes at the front of the Makran accretionary complex, Pakistan. Marine Geology, 172(1–2): 57–73

Whiticar M J. 1999. Carbon and hydrogen isotope systematics of bacterial formation and oxidation of methane. Chemical Geology, 161(1–3): 291–314

Wu Lushan, Yang Shengxiong, Liang Jinqiang, et al. 2013. Variations of pore water sulfate gradients in sediments as indicator for underlying gas hydrate in Shenhu Area, the South China Sea. Science China: Earth Sciences, 56(4): 530–540, doi: 10.1007/s11430-012-4545-6

Xu Cuiling, Wu Nengyou, Sun Zhilei, et al. 2018. Methane seepage inferred from pore water geochemistry in shallow sediments in the western slope of the Mid-Okinawa Trough. Marine and Petroleum Geology, 98: 306–315, doi: 10.1016j.marpetgeo./2018.08.021

Yang Tao, Jiang Shaoyong, Ge Lu, et al. 2013. Geochemistry of pore waters from HQ-1PC of the Qiongdongnan Basin, northern South China Sea, and its implications for gas hydrate exploration. Science China: Earth Sciences, 56(4): 521–529, doi: 10.1007/s11430-012-4560-7

Ye Hong, Yang Tao, Zhu Guorong, et al. 2016. Pore water geochemistry in shallow sediments from the northeastern continental slope of the South China Sea. Marine and Petroleum Geology, 75: 68–82, doi: 10.1016/j.marpetgeo.2016.03.010

Zhu Youhai, Huang Yongyang, Matsumoto R, et al. 2006. Geochemical and stable isotopic compositions of pore fluids and authigenic siderite concretions from Site 1146, ODP Leg 184: Implications for gas hydrate. In: Prell W L, Wang P, Blum P, et al., eds. Proceedings of the Ocean Drilling Program, 1–15